
Analysis of Atom-level pretraining with QM data for Graph Neural Networks Molecular property models

Jose Arjona-Medina
Janssen Research & Development
jarjonam@its.jnj.com

Ramil Nugmanov
Janssen Pharmaceutica NV
rnugmano@its.jnj.com

Abstract

Despite the rapid and significant advancements in deep learning for Quantitative Structure-Activity Relationship (QSAR) models, the challenge of learning robust molecular representations that effectively generalize in real-world scenarios to novel compounds remains an elusive and unresolved task. This study examines how atom-level pretraining with quantum mechanics (QM) data can mitigate violations of assumptions regarding the distributional similarity between training and test data and therefore improve performance and generalization in downstream tasks. In the public dataset Therapeutics Data Commons (TDC), we show how pretraining on atom-level QM improves performance overall and makes the activation of the features distributes more Gaussian-like which results in a representation that is more robust to distribution shifts. To the best of our knowledge, this is the first time that hidden state molecular representations are analyzed to compare the effects of molecule-level and atom-level pretraining on QM data.

1 Introduction

Despite the rapid and significant advancements in deep learning for Quantitative Structure-Activity Relationship (QSAR) models, the challenge of learning robust molecular representations that effectively generalize in real-world scenarios to novel compounds remains an elusive and unresolved task.

At the core of supervised learning with deep neural networks, there is the underlying assumption that the function we aim to approximate is "smooth" enough, meaning that small changes in the input should not result in large changes in the output [12]. However, in the application field of QSAR, we often experience regions where small chemical modifications drastically change the biological response [9]. For example, the extreme forms of Structure-Activity Relationship (SAR) discontinuity are called activity cliffs (AC) [1], which are formed by pairs of structurally similar compounds with large differences in potency [[32],[22]]. One way of overcoming this problem would be to increase the number of datapoints since the smoothness assumption works well as long as there are enough examples for the learning algorithm to observe high points on most peaks and low points on most valleys of the true underlying function to be learned [12]. However, it is not a general or scalable solution because the costs of producing additional experimental datapoints are high and would be applicable only locally for a specific target property

Supervised Learning methods also assume that test data comes from the same underlying distribution as training data [3]. Although novel techniques often present impressive metrics, most often they do not suffice to meet the practical needs in real-world drug discovery [10]. In the real world, data production is by construction strongly biased: Chemists work with structurally analogous series. In practice, target data is drifting [34], making these models obsolete for real-world production environments. The fundamental factors that influence molecular properties are still unexplored [10]. With statistical analyses, fixed representations like fingerprints generally match end-to-end deep

learning (DL) models in most datasets [10, 2, 26], especially in the presence of activity cliffs [35]. Much of the progress in molecular property estimation has been driven by the strategic incorporation of inductive biases [19, 38]. Techniques such as pretraining [39], the use of equivariant networks, and graph neural networks have proven useful [29, 17]. The shift towards leveraging domain-specific knowledge through inductive biases underlines the evolution in our approach to QSAR modeling.

Pretraining and Transfer Learning in QSAR Models. Pretraining has emerged as a potent solution to overcome data scarcity and enhance model generalizability in various domains, including image and natural language processing. However, without appropriate domain expertise, pretraining can sometimes lead to negative transfer or only marginal performance gains [27]. In the realm of molecular modeling, pretraining strategies have been successful, particularly when models are pretrained on large-scale datasets [36, 7, 33, 40]. For instance, the large-scale pretraining of models has been shown to improve sample efficiency in active learning frameworks used for molecule virtual screening [5]. Or [30] which enriches molecule representations with contextual knowledge from reference molecules using a Modern Hopfield Network [25]. Combining node-level and graph-level pre-training tasks to achieve superior generalization, particularly in out-of-distribution scenarios was presented in [14]. ChemBERTa utilizes large-scale pretraining datasets to explore the effects of dataset size on downstream task performance [7].

Multitask learning. Closely related to transfer learning, involves the simultaneous learning of multiple related tasks, enhancing the model’s ability to generalize across tasks [6]. This approach has been leveraged effectively in models like MolPMoFit, which was pretrained using bioactive molecules from ChEMBL for QSPR/QSAR tasks [19].

Multimodal and Self-supervised Learning. Recent advancements have also been made in multimodal learning and self-supervised learning frameworks. The GIMLET model, for example, pretrained on a dataset of molecule tasks with textual instructions, bridging the gap between graph and text data modalities and paving the way for instruction-based pretraining [44]. Similarly, the D&D framework utilizes a cross-modal distillation approach, transferring knowledge from 3D to 2D molecular structures, thereby significantly enhancing model performance in downstream tasks [8]. Or denoising 3D structures as a pre-training objective, setting new benchmarks in the widely used QM9 dataset [42].

Contrastive learning approaches [18, 16] can overcome data limitations by integrating additional data. For example, CLOOME [28] embeds bioimages and chemical structures into a unified space, enabling highly accurate retrieval of bioimages based on chemical structures. MolFeSCue [43] incorporates a dynamic contrastive loss function tailored for class imbalance. MolCLR [37] uses large-scale unlabeled data, graph-based augmentations, and a contrastive learning strategy to improve model generalization. A recent overview of methods for multi-modal contrastive learning is presented in [31].

Our approach effectively combines pretraining with QM data at node-level, to improve the downstream task of property modeling. We analyze the effect of this pretraining in the distribution of the features of the network, and we observe that atom-level pretrained networks have more Gaussian-like distributions which are more robust to distribution shifts in the input space, establishing a direct connection between pretraining at node-level and supervised learning theory of generalization.

Our contributions can be summarized as follows:

- We empirically show that atom-level pretraining in Graph neural networks with QM properties improves performance over scratch networks and molecular-level pretraining, in the TDC public dataset.
- We empirically show that atom-level pretraining produces a more normal distribution of features, compared to scratch and molecular-level pretrained networks.
- We empirically show that atom-level pretraining produces a more robust molecular representation against distribution shift from train to eval and train to test datasplits, which could explain the performance gain of atom-level pretraining approach.

To the best of our knowledge, this is the first study that aims to understand how atom-level pretraining improves molecular representation.

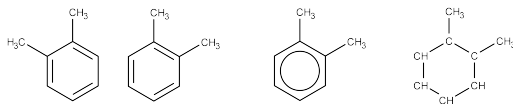


Figure 1: Different aromatic ring representations folded into a single form

2 Methods

Graphormer. In 2021, Microsoft published Graphormer[41], a neural network specifically engineered for processing graphs and, more pointedly, molecular structures. This network has exhibited outstanding performance in molecular quantum properties, adapting the architecture of BERT[11] to suit graph data effectively. Graphormer introduces several novel features, the key among them being "centrality encoding". This technique captures the importance of nodes within the graph by integrating graph degree centrality, which is encoded as embedding vectors added into the atom's node type embeddings. Additionally, Graphormer incorporates a "spatial encoding" strategy. This involves representing the shortest path between pairs of nodes, which is then utilized as a learnable bias in the attention matrix. This concept mirrors techniques used in other advanced models like T5[24] and ALIBI[23], highlighting its relevance and utility in enhancing the model's attention mechanism within graph networks.

Custom implementation. Following [21], we have refined the "centrality encoder" of the original Graphormer to encompass not just explicit neighbors but total neighbors, integrating both explicit atom neighbors and implicit hydrogens. This approach eliminates the need for an "edge encoder", leveraging a combination of the centrality encoder and an atom type encoder to implicitly capture atom hybridization. Moreover, we have streamlined the model by omitting the encoding of atoms' formal charges and radical states, allowing for the representation of resonance structures in a unified form and dispensing with the traditional concept of "aromatic" bonds typically applied to arenes. Additionally, our model introduces a "spatial encoder" constrained by a configurable maximum distance threshold to enhance computational efficiency and model accuracy. By treating distances beyond this threshold uniformly, the model focuses on more relevant short-range interactions understanding molecular structures.

Enabling multitask learning by task-specific virtual nodes. Similar to the original BERT model, Graphormer utilizes a [CLS] token as a global readout for estimating properties of graphs and molecules. This methodology aligns with techniques used in graph convolutional networks (GCNs), where virtual nodes connected to every node of the graph can serve a comparable purpose [4]. Building on this concept, we propose a novel extension tailored for multitask learning applications. In our approach, we employ the same encoder and output head to estimate multiple properties, but differentiate the tasks by using distinct virtual nodes for each. This allows for task-specific processing while maintaining a unified architecture, enhancing the model's efficiency, adaptability, and scalability in handling diverse learning tasks.

Quantitative Assessment of learned features. To analyze the impact of pretraining methods on the molecular representation captured by the model, we conducted a comprehensive analysis of learned feature distributions. We run the models on the three different data splits (training, validation, and test), and extract the distribution of features after the first layer of the Graphormer architecture.

For each compound in the dataset, we aggregated the node representations after the first Graphormer layer, resulting in a cumulative dataset-wide node representation. This aggregation facilitated the derivation of an empirical distribution of activations per model and data split. Using this empirical distribution, we applied various statistical techniques to quantify the differences in feature distributions across the different data splits for each of the models. Furthermore, we undertook an evaluation of the normality of these distributions using Shapiro-Wilk and Kolmogorov-Smirnov tests. This assessment was used to determine whether significant deviations exist in the distribution of learned features across different pretraining methods.

3 Experiments

Datasets For pretraining, we used a publicly available dataset [13] consisting of 136k organic molecules. Each molecule is represented by a single conformer generated using the Merck Molecular Force Field (MMFF94s) in the RDKit library. The initial geometry for the lowest-lying conformer was then optimized at the GFN2-xtb level of theory followed by refinement of the electronic structure with DFT (B3LYP/def2svp). The advantage of the described dataset is several reported atomic properties: charge, electrophilicity, nucleophilicity Fukui indexes, and an NMR shielding constant. Some additional curation was carried out as described in the addendum. Another pretraining dataset, PCQM4Mv2, consists of a single molecular property per molecule, a HOMO-LUMO gap <https://ogb.stanford.edu/docs/lsc/pcqm4mv2/>. It was curated under the PubChemQC project [20]. For the benchmarking of the obtained pretrained models, we used the absorption, distribution, metabolism, excretion, and toxicity (ADMET) group of the Therapeutics Data Commons (TDC) dataset [15], consisting of 9 regression and 13 binary classification tasks for modeling biochemical molecular properties.

Experiments setup We train our Graphormer network from scratch on the set of tasks provided by the TDC dataset. We also pretrained the same network using as main task HOMO-LUMO gap (molecule-level) and the atomic properties charge, electrophilicity, and nucleophilicity Fukui indexes and an NMR shielding constant (atom-level). For atom-level pretrain, we pretrained 4 models, one per every single property. We also pretrained a fifth model which is pretrained on 4 properties via multi-task by task-specific virtual nodes. Main results reported in this paper for atom-level uses this last model. Results for specific atomic property pretrained are available in the Supplementary Material.

4 Results

This section provides a concise summary of the key findings of this study. For an exhaustive elaboration of the results, please refer to the supplementary materials.

Pretraining on atom-level node with QM significantly improves performance in downstream tasks In Table 1, we present the outcomes from benchmarking three distinct training approaches: scratch, molecule-level QM pretrained, and atom-level QM pretrained with all properties for 5 different seeds, as described in the guidelines provided by the TDC dataset <https://tdcommons.ai/benchmark/overview/>. We have excluded the results for atom-level pretraining on individual QM properties from this table; these can be found in the Supplementary Materials. These results show that atom-level pretraining notably enhances model performance compared to training from scratch for 21 of the 22 datasets.

Pretraining on atom-level node with QM results on smoother feature distribution We further examined the distribution of the features from the network’s first layer for atom-level pretrained, molecular-level (HOMO-LUMO gap) and scratch models across different data splits and datasets. Figure 2 illustrates the feature distribution for the test split of one of the datasets (lipophilicity), highlighting how scratch and molecular-level pretrain compare to the atom-level pretrained network (for other datasets and splits, please refer to the Supplementary Materials). Visually, we can observe that the atom-level pretrained method results in a more Gaussian-like distribution of the features. We conducted a Shapiro-Wilk test for each dimension in both scratch and pretrained networks to assess the normality of the distributions. The average p-value for the scratch network was $3.2E-06$ with a standard deviation of $5E-05$, suggesting a significant deviation from normality. In contrast, the pretrained network had an average p-value of $4E-04$ with a standard deviation of 0.003, indicating a closer approximation to a Gaussian distribution.

Pretraining on atom-level node with QM enhances robustness to input distribution shifts Pretrained networks show in general less distribution shift compared to scratch network, as we can see in Figure 3. In this figure, we show the distribution shifts differences between scratch and pretrained networks. As we can appreciate, in most of the cases, specially in the Train-Test comparison, atom-level pretrained networks have less distribution shift than scratch networks.

Table 1: Graphormer results

	Metric	Direction	scratch	mol-level pretrained HLgap	atom-level pretrained all (4)
caco2_wang	MAE	↓	0.48 ± 0.06	0.53 ± 0.02	0.41 ± 0.03
lipophilicity_astrazeneca	MAE	↓	0.58 ± 0.02	0.57 ± 0.02	0.42 ± 0.01
solubility_aqsoldb	MAE	↓	0.89 ± 0.04	0.89 ± 0.02	0.75 ± 0.01
ppbr_az	MAE	↓	8.38 ± 0.24	8.22 ± 0.23	7.79 ± 0.24
ld50_zhu	MAE	↓	0.61 ± 0.02	0.60 ± 0.03	0.57 ± 0.02
hia_hou	ROC-AUC	↑	0.96 ± 0.03	0.96 ± 0.02	0.94 ± 0.05
pgp_broccatelli	ROC-AUC	↑	0.87 ± 0.04	0.86 ± 0.01	0.89 ± 0.02
bioavailability_ma	ROC-AUC	↑	0.52 ± 0.01	0.55 ± 0.03	0.64 ± 0.05
bbb_martins	ROC-AUC	↑	0.83 ± 0.01	0.82 ± 0.03	0.88 ± 0.02
cyp3a4_substrate_carbonmangels	ROC-AUC	↑	0.63 ± 0.07	0.64 ± 0.03	0.64 ± 0.02
ames	ROC-AUC	↑	0.72 ± 0.02	0.73 ± 0.01	0.80 ± 0.01
dili	ROC-AUC	↑	0.86 ± 0.02	0.87 ± 0.01	0.88 ± 0.03
herg	ROC-AUC	↑	0.78 ± 0.01	0.76 ± 0.04	0.77 ± 0.06
vdss_lombardo	Spearman	↑	0.58 ± 0.04	0.59 ± 0.04	0.59 ± 0.03
half_life_obach	Spearman	↑	0.39 ± 0.07	0.34 ± 0.07	0.48 ± 0.06
clearance_microsome_az	Spearman	↑	0.49 ± 0.03	0.46 ± 0.03	0.60 ± 0.01
clearance_hepatocyte_az	Spearman	↑	0.34 ± 0.04	0.31 ± 0.02	0.46 ± 0.03
cyp2d6_veith	PR-AUC	↑	0.43 ± 0.03	0.47 ± 0.02	0.61 ± 0.02
cyp3a4_veith	PR-AUC	↑	0.73 ± 0.01	0.74 ± 0.03	0.80 ± 0.03
cyp2c9_veith	PR-AUC	↑	0.63 ± 0.02	0.66 ± 0.03	0.69 ± 0.02
cyp2d6_substrate_carbonmangels	PR-AUC	↑	0.52 ± 0.01	0.54 ± 0.04	0.58 ± 0.03
cyp2c9_substrate_carbonmangels	PR-AUC	↑	0.35 ± 0.02	0.33 ± 0.03	0.37 ± 0.04

Distribution of Activations for 20 Features

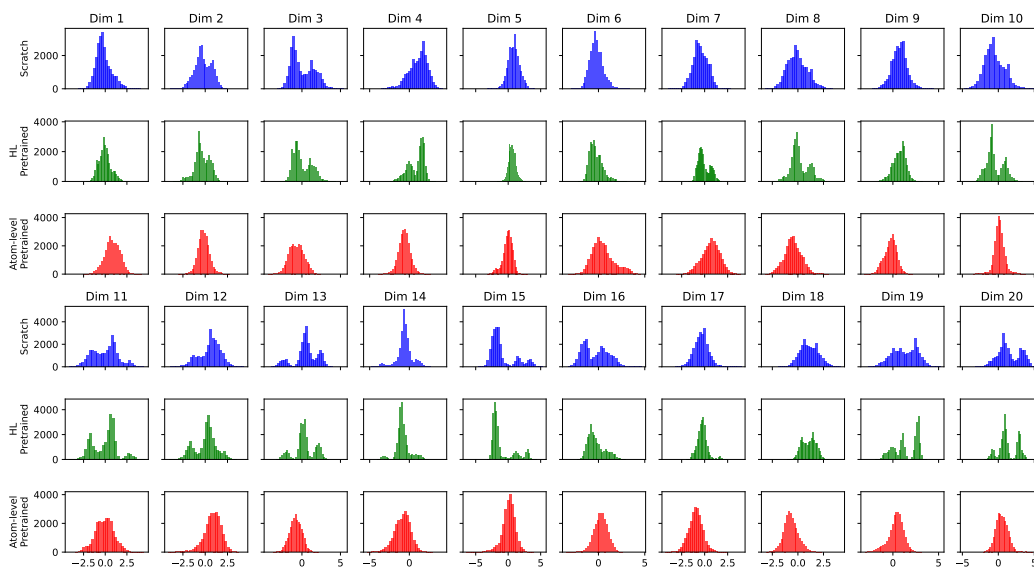


Figure 2: Distribution of first 20 features from the first layer of the Graphormer network for three different training approaches —scratch, HOMO-LUMO pretrained and atom-level pretrained— across test split of lipophilicity dataset .

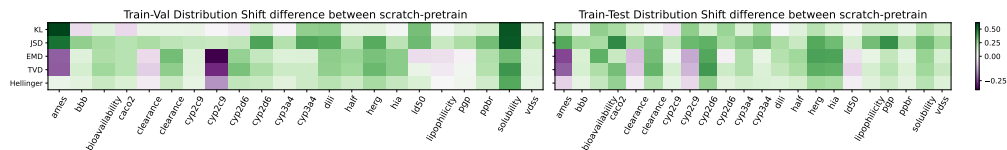


Figure 3: This heatmap illustrates the differences in distribution shifts between scratch and atom-level pretrained networks, calculated across various feature dimensions using metrics such as Kullback-Leibler Divergence, Jensen-Shannon Divergence, Earth Mover’s Distance, Total Variation Distance, and Hellinger Distance. Green hues indicate instances where the atom-level pretrained network exhibits smaller distribution shifts compared to the scratch network, while purple hues denote the opposite. Notably, both heatmaps comparison frequently show reduced distribution shifts in atom-level pretrained networks, specially for Train-Test comparison, which likely helps to explain atom-level pretrained network’s superior performance on the test data split.

5 Conclusions

In this study, we have demonstrated that pretraining of graph-based neural networks with atom-level quantum mechanics (QM) data significantly enhances performance on downstream tasks related to ADMET properties within the TDC dataset, as illustrated in Table 1. Furthermore, we showed the change in the distributions of activations of the internal model’s features due to specific pretraining. After atom-level pretraining with QM data, these distributions become more Gaussian-like, which is known to be conducive to better learning dynamics and thus improved performance (see Figure 2). Moreover, our findings indicate that pretrained models exhibit smaller distribution shifts from training to testing datasets, further supporting the efficacy of QM data pretraining in enhancing model robustness (see Figure 2).

To our knowledge, this is the first study that elucidates how atom-level pretraining can optimize molecular representations by analyzing the model’s internal representation and robustness to distribution shifts.

References

- [1] J. Bajorath, L. Peltason, M. Wawer, R. Guha, M. S. Lajiness, and J. H. Van Drie. Navigating structure-activity landscapes. *Drug Discov Today*, 14(13-14):698–705, 2009.
- [2] D. Baptista, J. Correia, B. Pereira, and M. Rocha. Evaluating molecular representations in machine learning models for drug response prediction and interpretability. *J Integr Bioinform*, 19(3):20220006, 2022.
- [3] C. M. Bishop. *Pattern Recognition and Machine Learning*. Springer, 2006.
- [4] C. Cai, T. S. Hy, R. Yu, and Y. Wang. On the connection between mpnn and graph transformer. In *Proceedings of the 40th International Conference on Machine Learning*, page 138. JMLR.org, 2023.
- [5] Z. Cao, S. Sciabola, and Y. Wang. Large-scale pretraining improves sample efficiency of active learning based molecule virtual screening. In *The NeurIPS 2023 Workshop on New Frontiers of AI for Drug Discovery and Development (AI4D3 2023)*, 2023.
- [6] R. Caruana. Multitask learning. *Machine Learning*, 28(1):41–75, 1997.
- [7] S. Chithrananda, G. Grand, and B. Ramsundar. Chemberta: Large-scale self-supervised pretraining for molecular property prediction, 2020.
- [8] S. Cho, D.-W. Jeong, S. M. Ko, J. Kim, S. Han, S. Hong, H. Lee, and M. Lee. 3d denoisers are good 2d teachers: Molecular pretraining via denoising and cross-modal distillation, 2023.
- [9] M. Cruz-Monteagudo, J. L. Medina-Franco, Y. Pérez-Castillo, O. Nicolotti, M. N. D. S. Cordeiro, and F. Borges. Activity cliffs in drug discovery: Dr jekyll or mr hyde? *Drug Discovery Today*, 19(8):1069–1080, 2014.
- [10] J. Deng, Z. Yang, and H. Wang et al. A systematic study of key elements underlying molecular property prediction. *Nat Commun*, 14:6395, 2023.

- [11] J. Devlin, M. W. Chang, K. Lee, and K. Toutanova. Bert: Pre-training of deep bidirectional transformers for language understanding. In *Proc. Conference of the North American Chapter of the Association for Computational Linguistics: Human Language Technologies (NAACL-HLT)*, pages 4171–4186, 2019.
- [12] Ian Goodfellow, Yoshua Bengio, and Aaron Courville. *Deep Learning*. MIT Press, 2016. <http://www.deeplearningbook.org>.
- [13] Yanfei Guan, Connor W. Coley, Haoyang Wu, Duminda Ranasinghe, Esther Heid, Thomas J. Struble, Lagnajit Pattanaik, William H. Green, and Klavs F. Jensen. Regio-selectivity prediction with a machine-learned reaction representation and on-the-fly quantum mechanical descriptors. *Chemical Science*, 12(6):2198–2208, 2021.
- [14] W. Hu, B. Liu, J. Gomes, M. Zitnik, P. Liang, V. Pande, and J. Leskovec. Strategies for pre-training graph neural networks, 2020.
- [15] Kexin Huang, Tianfan Fu, Wenhao Gao, Yue Zhao, Yusuf Roohani, Jure Leskovec, Connor W. Coley, Cao Xiao, Jimeng Sun, and Marinka Zitnik. Artificial intelligence foundation for therapeutic science. *Nature Chemical Biology*, 18(10):1033–1036, 2022.
- [16] Prannay Khosla, Piotr Teterwak, Chen Wang, Aaron Sarna, Yonglong Tian, Phillip Isola, Aaron Maschiot, Ce Liu, and Dilip Krishnan. Supervised contrastive learning. In H. Larochelle, M. Ranzato, R. Hadsell, M.F. Balcan, and H. Lin, editors, *Advances in Neural Information Processing Systems*, volume 33, pages 18661–18673. Curran Associates, Inc., 2020.
- [17] T. Le, F. Noé, and D. Clevert. Equivariant graph attention networks for molecular property prediction. In *Proceedings of the Learning on Graphs Conference 2022*. LoG Conference, 2022.
- [18] Phuc H. Le-Khac, Graham Healy, and Alan F. Smeaton. Contrastive representation learning: A framework and review. *IEEE Access*, 8:193907–193934, 2020.
- [19] X. Li and D. Fourches. Inductive transfer learning for molecular activity prediction: Next-gen qsar models with molpmofit. *J Cheminform*, page 27, 2020.
- [20] Maho Nakata and Tomomi Shimazaki. PubChemQC Project: A Large-Scale First-Principles Electronic Structure Database for Data-Driven Chemistry. *Journal of Chemical Information and Modeling*, 57(6):1300–1308, 2017.
- [21] R. Nugmanov, N. Dyubankova, A. Gedich, and J. K. Wegner. Bidirectional graphormer for reactivity understanding: Neural network trained to reaction atom-to-atom mapping task. *Journal of Chemical Information and Modeling*, 62(14):3307–3315, 2022.
- [22] L. Peltason and J. Bajorath. *Computational Analysis of Activity and Selectivity Cliffs*, volume 672, pages 119–132. Humana Press, 2011.
- [23] O. Press, N. A. Smith, and M. Lewis. Train short, test long: Attention with linear biases enables input length extrapolation. In *Proc. Annual Meeting of the Association for Computational Linguistics*. ACL, 2021.
- [24] C. Raffel, N. Shazeer, A. Roberts, K. Lee, S. Narang, M. Matena, Y. Zhou, W. Li, and P. J. Liu. Exploring the limits of transfer learning with a unified text-to-text transformer. In *Proc. Annual Conference on Neural Information Processing Systems (NeurIPS)*, 2019.
- [25] Hubert Ramsauer, Bernhard Schöfl, Johannes Lehner, Philipp Seidl, Michael Widrich, Thomas Adler, Lukas Gruber, Markus Holzleitner, Milena Pavlović, Geir Kjetil Sandve, Victor Greiff, David Kreil, Michael Kopp, Günter Klambauer, Johannes Brandstetter, and Sepp Hochreiter. Hopfield networks is all you need. In *International Conference on Learning Representations*, 2021.
- [26] M. C. Robinson, R. C. Glen, and A. A. Lee. Validating the validation: reanalyzing a large-scale comparison of deep learning and machine learning models for bioactivity prediction. *J Comput Aided Mol Des*, 34:717–730, 2020.
- [27] M. T. Rosenstein, Z. Marx, L. P. Kaelbling, and T. G. Dietterich. To transfer or not to transfer. In *Advances in Neural Information Processing Systems (NeurIPS), Workshop on transfer learning*, volume 898, pages 1–4, 2005.
- [28] A. Sanchez-Fernandez, E. Rumetshofer, and S. Hochreiter et al. Cloome: contrastive learning unlocks bioimaging databases for queries with chemical structures. *Nat Commun*, 14:7339, 2023.

- [29] V. Garcia Satorras, E. Hoogeboom, and M. Welling. E(n) equivariant graph neural networks. In *Proceedings of the International Conference on Learning Representations (ICLR)*, 2021.
- [30] Johannes Schimunek, Philipp Seidl, Lukas Friedrich, Daniel Kuhn, Friedrich Rippmann, Sepp Hochreiter, and Günter Klambauer. Context-enriched molecule representations improve few-shot drug discovery. In *The Eleventh International Conference on Learning Representations*, 2023.
- [31] Philipp Seidl. *Multimodal Contrastive Learning for Drug Discovery*. Dissertation (phd), Johannes Kepler University Linz, Linz, 2024. Includes illustrations.
- [32] D. Stumpfe and J. Bajorath. Exploring activity cliffs in medicinal chemistry miniperspective. *Journal of Medicinal Chemistry*, 55(7):2932–2942, 2012.
- [33] H. Stärk, D. Beaini, G. Corso, P. Tossou, C. Dallago, S. Günnemann, and P. Lió. 3d infomax improves gnn for molecular property prediction. In *Proceedings of the 39th International Conference on Machine Learning (ICML)*. PMLR, 2023.
- [34] P. Tossou, C. Wognum, M. Craig, M. H., and E. Noutahi. Real-world molecular out-of-distribution: Specification and investigation. *ChemRxiv*, 2023. This content is a preprint and has not been peer-reviewed.
- [35] D. van Tilborg, A. Alenicheva, and F. Grisoni. Exposing the limitations of molecular machine learning with activity cliffs. *Journal of Chemical Information and Modeling*, 62(23):5938–5951, 2022.
- [36] S. Wang, Y. Guo, Y. Wang, H. Sun, and J. Huang. Smiles-bert: Large scale unsupervised pre-training for molecular property prediction. In *Proceedings of the 10th ACM International Conference on Bioinformatics, Computational Biology and Health Informatics (ACM-BCB)*, pages 429–436, Niagara Falls, NY, USA, 2019. ACM.
- [37] Yuyang Wang, Jianren Wang, Zhonglin Cao, and Amir Barati Farimani et al. Molecular contrastive learning of representations via graph neural networks. *Nat Mach Intell*, 4:279–287, 2022.
- [38] J. Xia, L. Zhang, X. Zhu, Y. Liu, Z. Gao, B. Hu, C. Tan, J. Zheng, S. Li, and S. Z. Li. Understanding the limitations of deep models for molecular property prediction: Insights and solutions. In *Advances in Neural Information Processing Systems*, volume 36, pages 64774–64792. Curran Associates, Inc., 2023.
- [39] J. Xia, Y. Zhu, Y. Du, and S. Z. Li. A systematic survey of chemical pre-trained models. In *Proceedings of the Thirty-Second International Joint Conference on Artificial Intelligence (IJCAI-23)*. IJCAI, 2023.
- [40] L. Xu, L. Xia, S. Pan, and Z. Li. Triple generative self-supervised learning method for molecular property prediction. *Int. J. Mol. Sci.*, 25(7):3794, 2024.
- [41] C. Ying, T. Cai, S. Luo, S. Zheng, G. Ke, D. He, Y. Shen, and T.-Y. Liu. Do transformers really perform badly for graph representation? In M. Ranzato, A. Beygelzimer, Y. Dauphin, P. S. Liang, and J. Wortman Vaughan, editors, *Advances in Neural Information Processing Systems*, volume 34, pages 28877–28888. Curran Associates, Inc., 2021.
- [42] S. Zaidi, M. Schaarschmidt, J. Martens, H. Kim, Y. W. Teh, A. Sanchez-Gonzalez, P. Battaglia, R. Pascanu, and J. Godwin. Pre-training via denoising for molecular property prediction, 2022.
- [43] Ruochi Zhang, Chao Wu, Qian Yang, Chang Liu, Yan Wang, Kewei Li, Lan Huang, and Fengfeng Zhou. Molfescue: enhancing molecular property prediction in data-limited and imbalanced contexts using few-shot and contrastive learning. *Bioinformatics*, 40:btac118, 2024.
- [44] H. Zhao, S. Liu, C. Ma, H. Xu, J. Fu, Z.-H. Deng, L. Kong, and Q. Liu. Gimlet: A unified graph-text model for instruction-based molecule zero-shot learning, 2023.

A Supplementary Materials

A.1 Full table results

A.2 Distribution of activations of features for scratch, HOMO-LUMO pretrained and Atom-level pretrained networks in TDC Lipophilicity Dataset

A.3 Distribution of first 20 features from the first layer of the Graphormer network for three different training approaches —scratch, HOMO-LUMO pretrained and atom-level pretrained— across test split of TDC datasets

Table 2: Graphormer results

	Metric	Direction	scratch	HL_gap	atom-level pretrained all (4)	fukui_e	nmr	fukui_n	charge	mol-level pretrained HL_gap
caco2_wang	MAE	↓	0.48 ± 0.06	0.53 ± 0.02	0.41 ± 0.03	0.45 ± 0.07	0.48 ± 0.06	0.39 ± 0.02	0.40 ± 0.08	0.53 ± 0.02
	lipophilicity_astrazeneca	↓	0.58 ± 0.02	0.57 ± 0.02	0.42 ± 0.01	0.49 ± 0.02	0.46 ± 0.01	0.48 ± 0.01	0.43 ± 0.01	0.57 ± 0.02
	solubility_aqsoldb	↓	0.89 ± 0.04	0.89 ± 0.02	0.75 ± 0.01	0.80 ± 0.02	0.78 ± 0.02	0.78 ± 0.02	0.75 ± 0.01	0.89 ± 0.02
	ppbr_az	↓	8.38 ± 0.24	8.22 ± 0.23	7.79 ± 0.24	7.92 ± 0.12	8.02 ± 0.40	7.79 ± 0.28	7.57 ± 0.32	8.22 ± 0.23
	ld50_zhu	↓	0.61 ± 0.02	0.60 ± 0.03	0.57 ± 0.02	0.60 ± 0.01	0.56 ± 0.02	0.60 ± 0.02	0.57 ± 0.01	0.60 ± 0.03
hia_hou	ROC-AUC	↑	0.96 ± 0.03	0.96 ± 0.02	0.94 ± 0.05	0.93 ± 0.03	0.97 ± 0.02	0.94 ± 0.02	0.95 ± 0.02	0.96 ± 0.02
	ROC-AUC	↑	0.87 ± 0.04	0.86 ± 0.01	0.89 ± 0.02	0.89 ± 0.03	0.86 ± 0.03	0.90 ± 0.01	0.88 ± 0.02	0.86 ± 0.01
	ROC-AUC	↑	0.52 ± 0.01	0.55 ± 0.03	0.64 ± 0.05	0.64 ± 0.02	0.66 ± 0.01	0.69 ± 0.05	0.62 ± 0.07	0.55 ± 0.03
	bbb_martins	↑	0.83 ± 0.01	0.82 ± 0.03	0.88 ± 0.02	0.86 ± 0.03	0.86 ± 0.02	0.85 ± 0.02	0.87 ± 0.01	0.82 ± 0.03
	cyp3a4_substrate_carbonmangels	↑	0.63 ± 0.07	0.64 ± 0.03	0.64 ± 0.02	0.66 ± 0.03	0.62 ± 0.02	0.61 ± 0.02	0.63 ± 0.02	0.64 ± 0.03
	ames	↑	0.72 ± 0.02	0.73 ± 0.01	0.80 ± 0.01	0.78 ± 0.02	0.80 ± 0.02	0.76 ± 0.01	0.80 ± 0.01	0.73 ± 0.01
	dili	↑	0.86 ± 0.02	0.87 ± 0.01	0.88 ± 0.03	0.86 ± 0.04	0.89 ± 0.03	0.82 ± 0.04	0.85 ± 0.04	0.87 ± 0.01
	herg	↑	0.78 ± 0.01	0.76 ± 0.04	0.77 ± 0.06	0.73 ± 0.06	0.77 ± 0.05	0.77 ± 0.02	0.79 ± 0.03	0.76 ± 0.04
vdss_lombardo	Spearman	↑	0.58 ± 0.04	0.59 ± 0.04	0.59 ± 0.03	0.64 ± 0.02	0.61 ± 0.04	0.61 ± 0.01	0.63 ± 0.03	0.59 ± 0.04
	half_life_obach	↑	0.39 ± 0.07	0.34 ± 0.07	0.48 ± 0.06	0.48 ± 0.04	0.42 ± 0.10	0.48 ± 0.03	0.47 ± 0.04	0.34 ± 0.07
	clearance_microsome_az	↑	0.49 ± 0.03	0.46 ± 0.03	0.60 ± 0.01	0.47 ± 0.06	0.57 ± 0.01	0.58 ± 0.02	0.58 ± 0.01	0.46 ± 0.03
	clearance_hepatocyte_az	↑	0.34 ± 0.04	0.31 ± 0.02	0.46 ± 0.03	0.42 ± 0.02	0.44 ± 0.04	0.41 ± 0.02	0.46 ± 0.04	0.31 ± 0.02
cyp2d6_veith	PR-AUC	↑	0.43 ± 0.03	0.47 ± 0.02	0.61 ± 0.02	0.55 ± 0.03	0.56 ± 0.04	0.56 ± 0.02	0.58 ± 0.04	0.47 ± 0.02
	cyp3a4_veith	↑	0.73 ± 0.01	0.74 ± 0.03	0.80 ± 0.03	0.77 ± 0.03	0.78 ± 0.01	0.79 ± 0.03	0.76 ± 0.04	0.74 ± 0.03
	cyp2c9_veith	↑	0.63 ± 0.02	0.66 ± 0.03	0.69 ± 0.02	0.67 ± 0.02	0.69 ± 0.04	0.69 ± 0.01	0.69 ± 0.02	0.66 ± 0.03
	cyp2d6_substrate_carbonmangels	↑	0.52 ± 0.01	0.54 ± 0.04	0.58 ± 0.03	0.53 ± 0.06	0.64 ± 0.06	0.57 ± 0.04	0.63 ± 0.03	0.54 ± 0.04
	cyp2c9_substrate_carbonmangels	↑	0.35 ± 0.02	0.33 ± 0.03	0.37 ± 0.04	0.32 ± 0.04	0.34 ± 0.03	0.37 ± 0.04	0.36 ± 0.04	0.33 ± 0.03

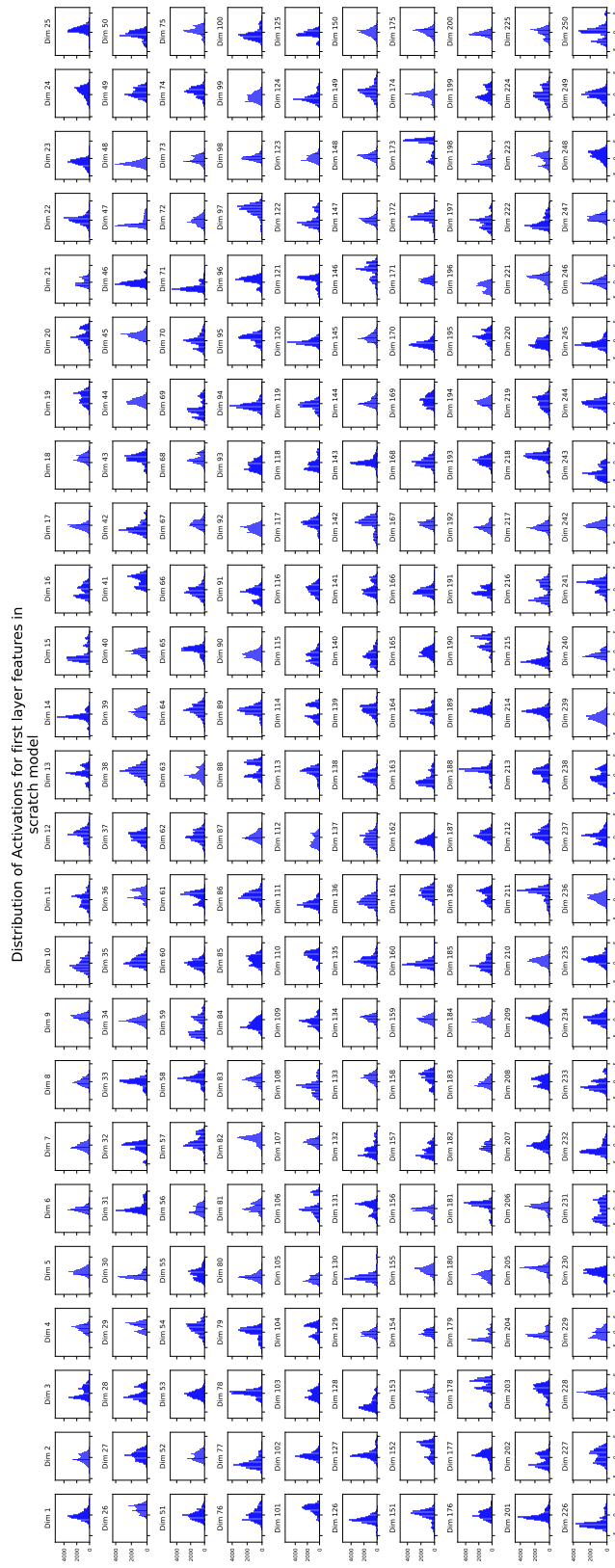


Figure 4: Distribution plots Scratch for Lipophilicity test set

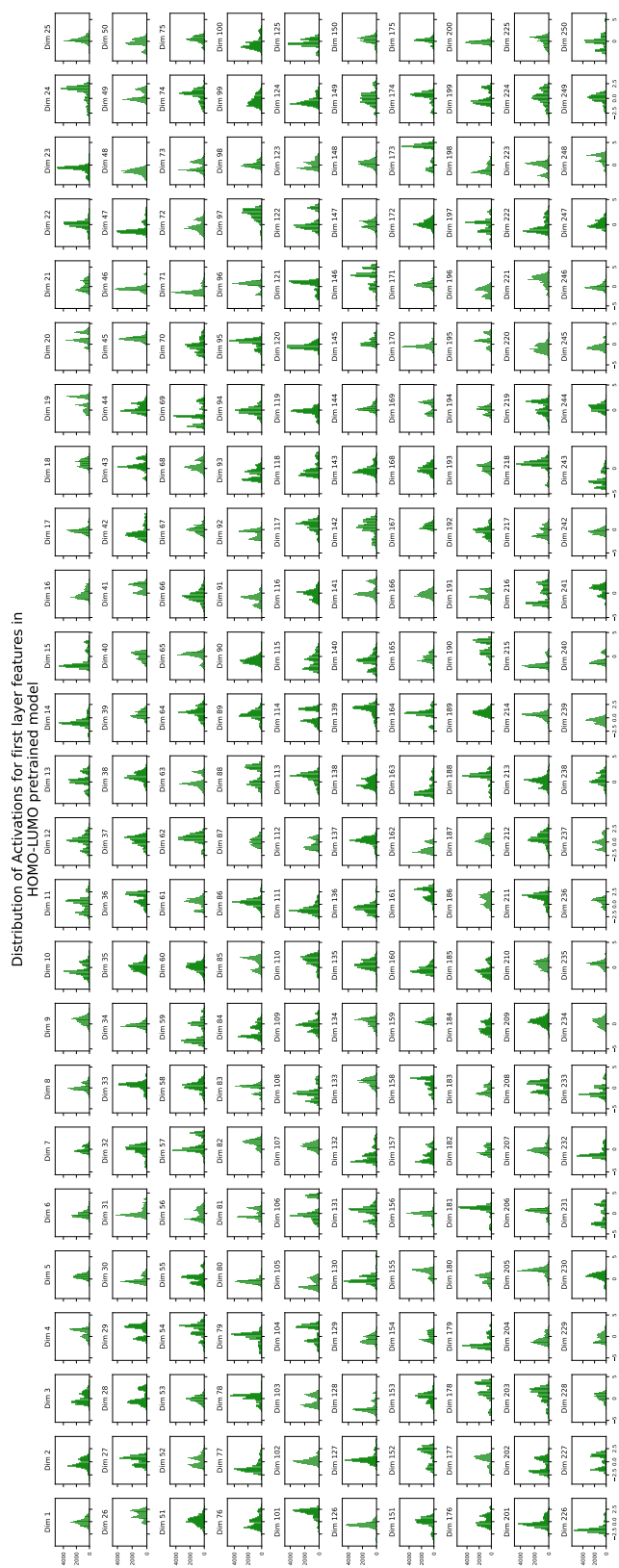


Figure 5: Distribution plots HOMO-LUMO pretrained for Lipophilicity test set

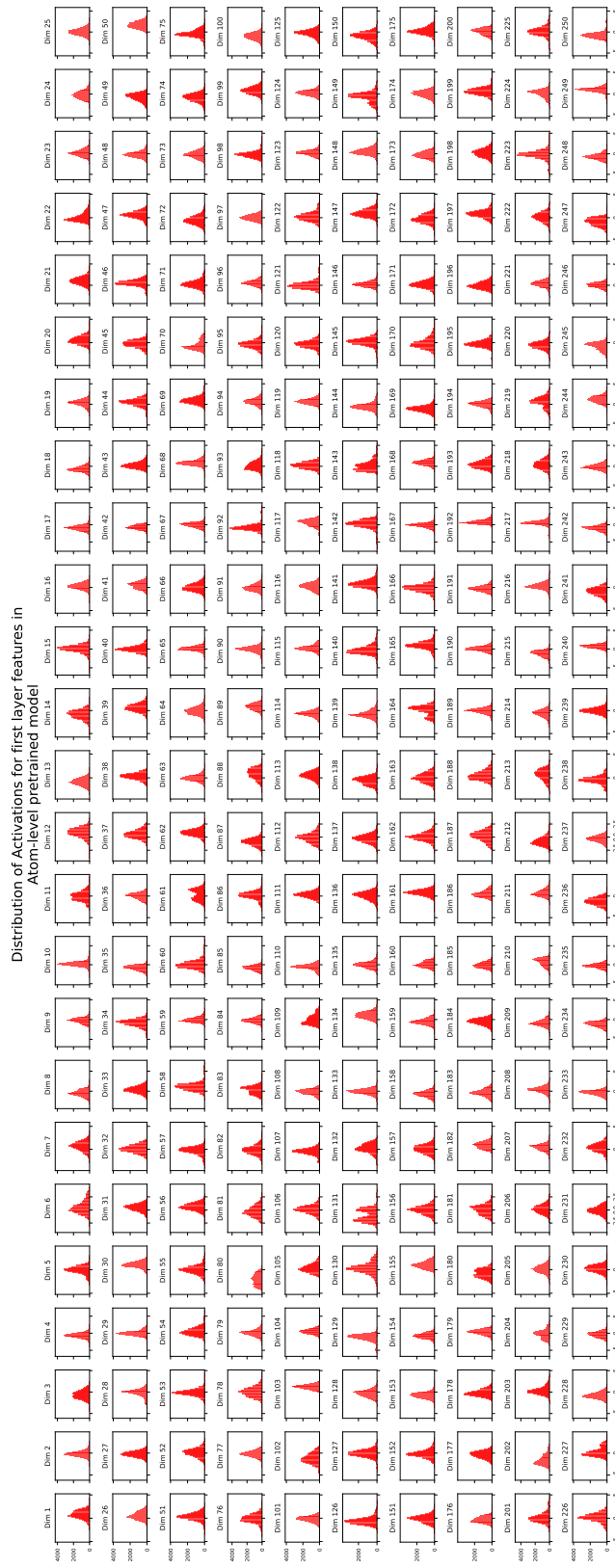


Figure 6: Distribution plots Atom-level pretrained for Lipophilicity test set

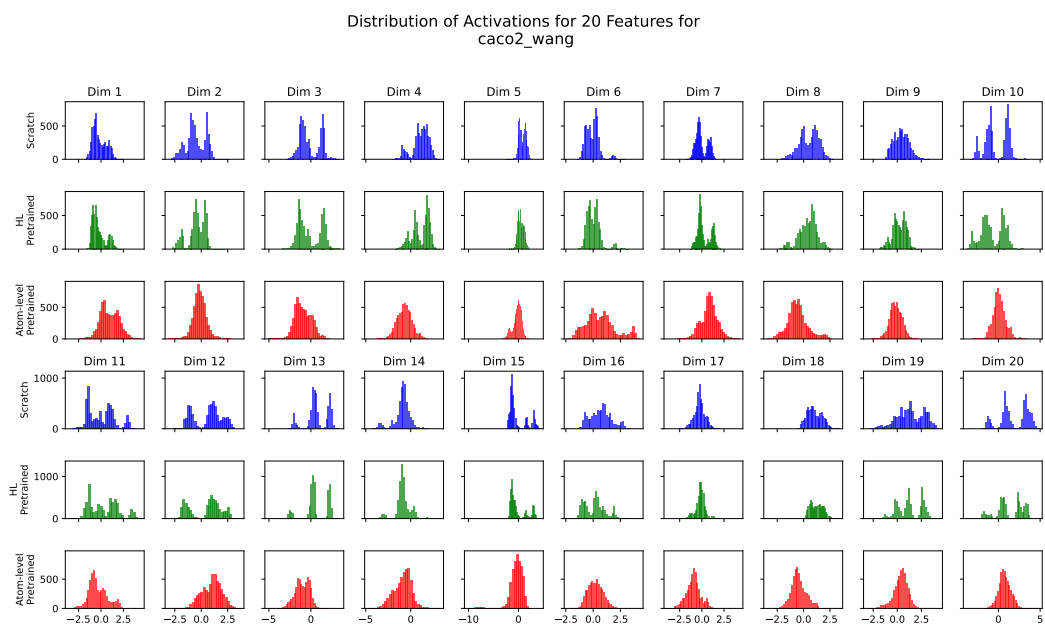


Figure 7: Distribution of first 20 features from the first layer of the Graphormer network for three different training approaches —scratch, HOMO-LUMO pretrained and atom-level pretrained— across test split of caco2 wang dataset.

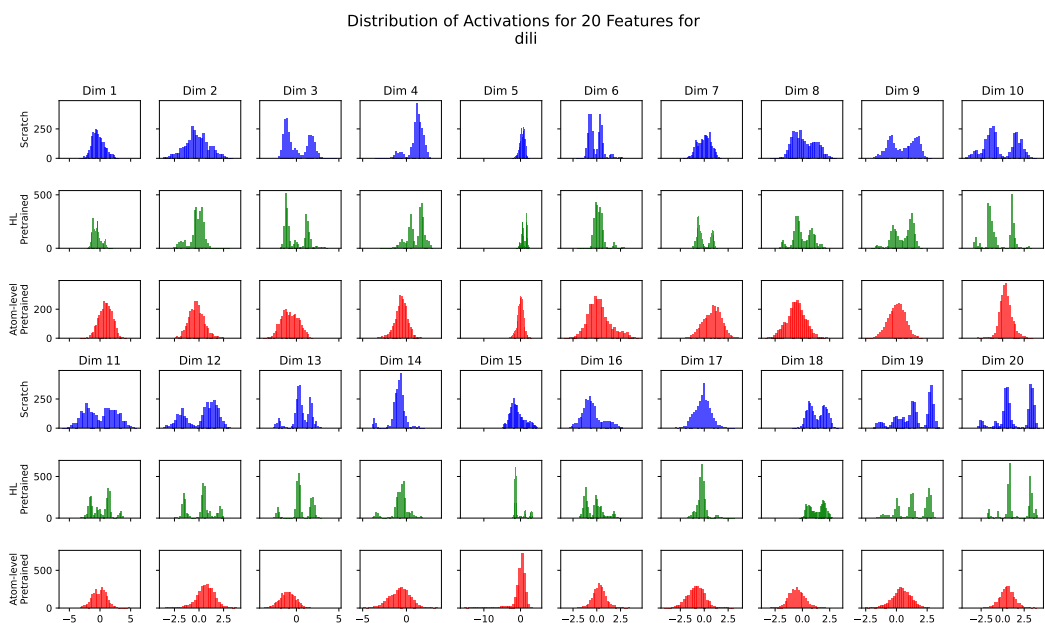


Figure 8: Distribution of first 20 features from the first layer of the Graphormer network for three different training approaches —scratch, HOMO-LUMO pretrained and atom-level pretrained— across test split of dili dataset.

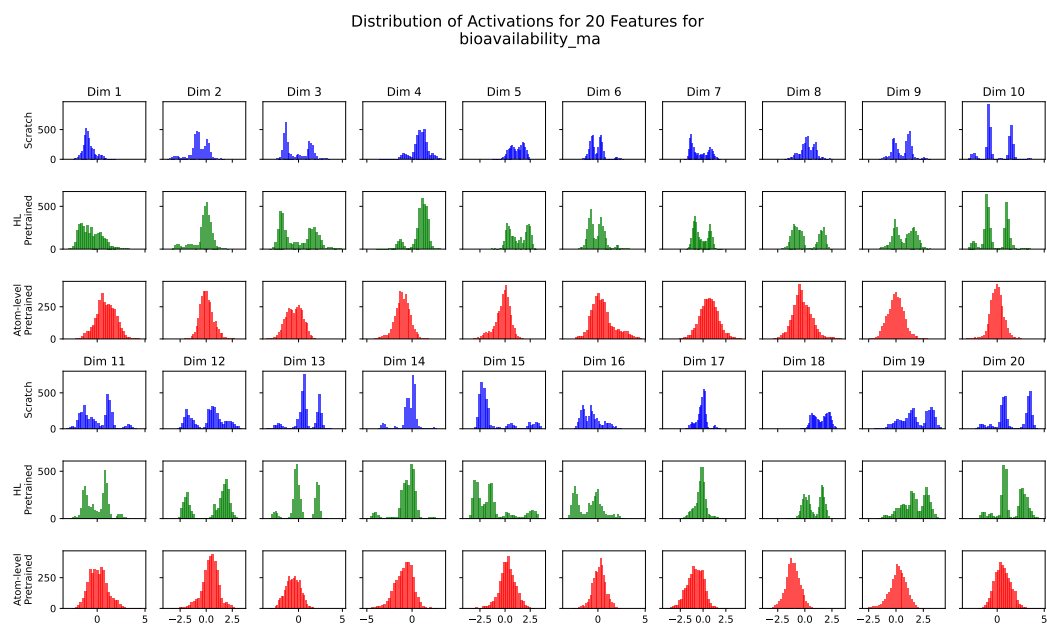


Figure 9: Distribution of first 20 features from the first layer of the Graphormer network for three different training approaches —scratch, HOMO-LUMO pretrained and atom-level pretrained— across test split of bioavailability ma dataset.

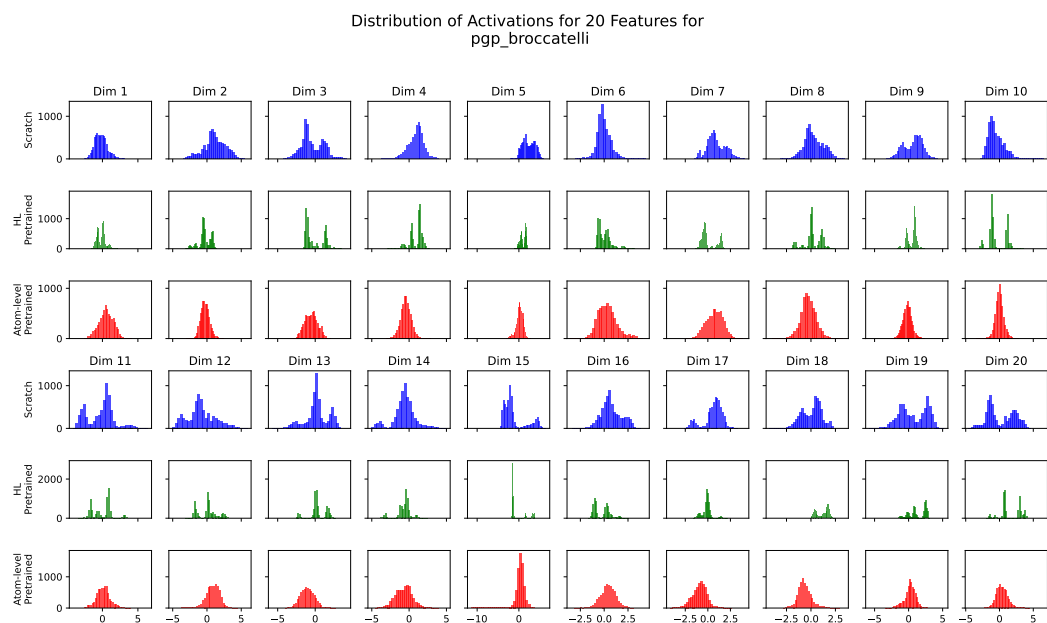


Figure 10: Distribution of first 20 features from the first layer of the Graphormer network for three different training approaches —scratch, HOMO-LUMO pretrained and atom-level pretrained— across test split of pgp broccatelli dataset.



Figure 11: Distribution of first 20 features from the first layer of the Graphormer network for three different training approaches —scratch, HOMO-LUMO pretrained and atom-level pretrained— across test split of ames dataset.

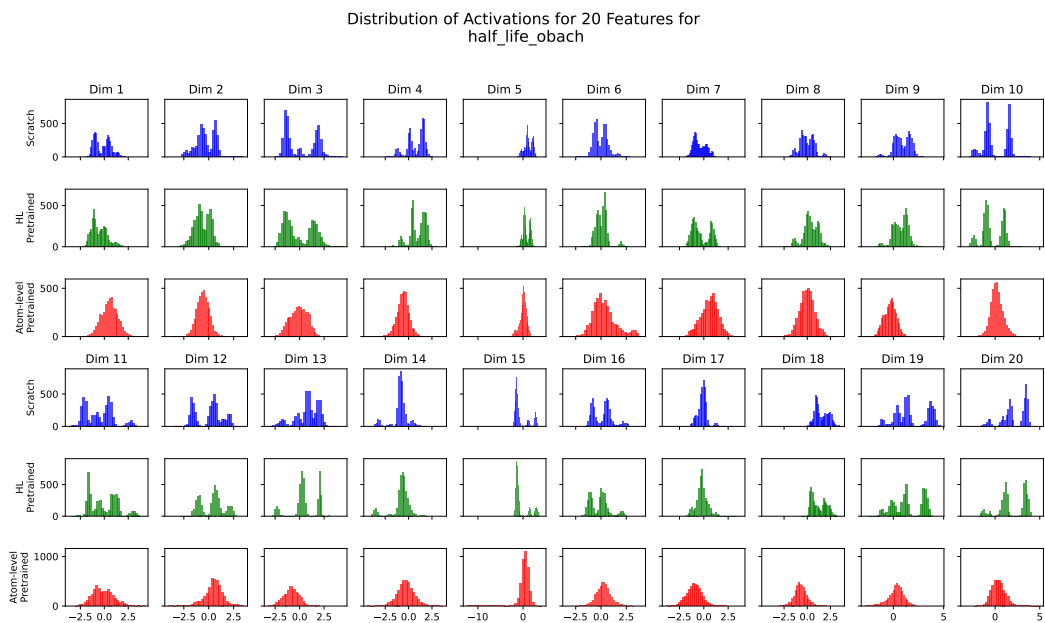


Figure 12: Distribution of first 20 features from the first layer of the Graphormer network for three different training approaches —scratch, HOMO-LUMO pretrained and atom-level pretrained— across test split of half life obach dataset.



Figure 13: Distribution of first 20 features from the first layer of the Graphormer network for three different training approaches —scratch, HOMO-LUMO pretrained and atom-level pretrained— across test split of herg dataset.

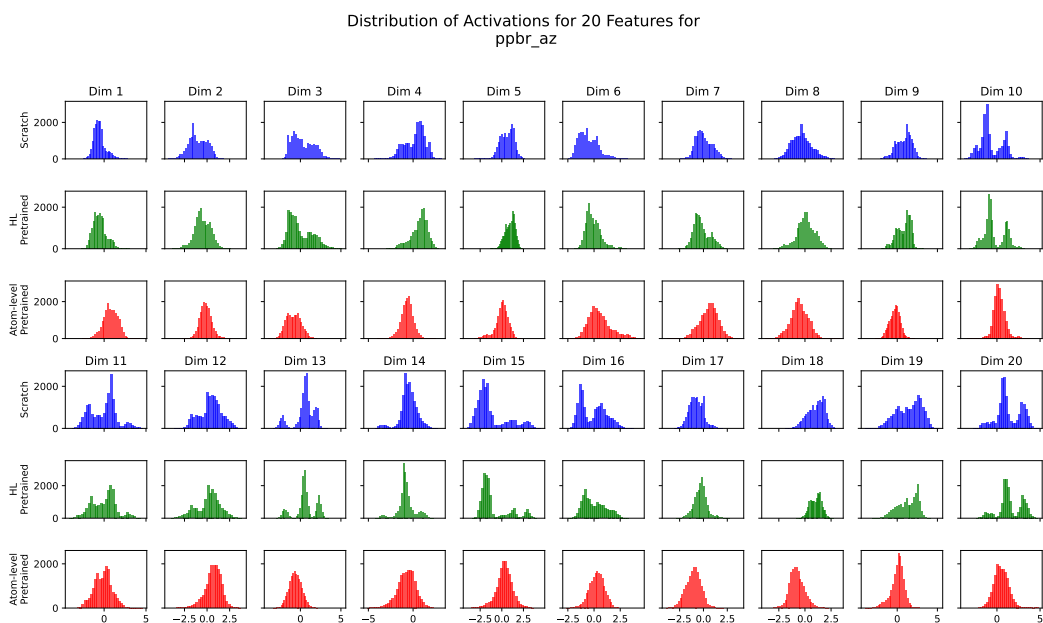


Figure 14: Distribution of first 20 features from the first layer of the Graphormer network for three different training approaches —scratch, HOMO-LUMO pretrained and atom-level pretrained— across test split of pbr az dataset.

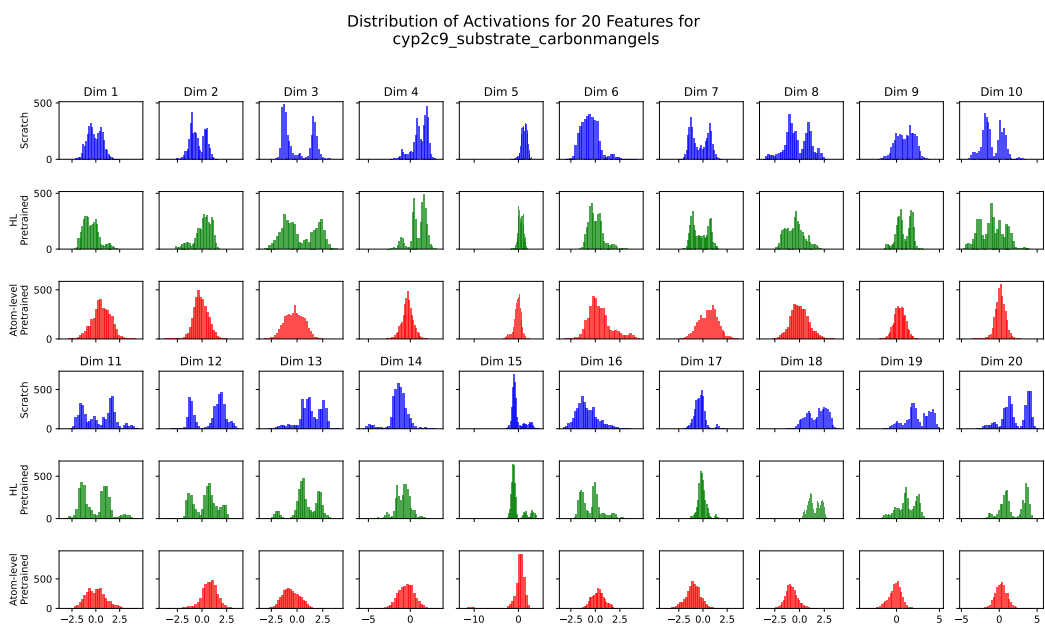


Figure 15: Distribution of first 20 features from the first layer of the Graphormer network for three different training approaches —scratch, HOMO-LUMO pretrained and atom-level pretrained— across test split of cyp2c9 substrate carbonmangels dataset.

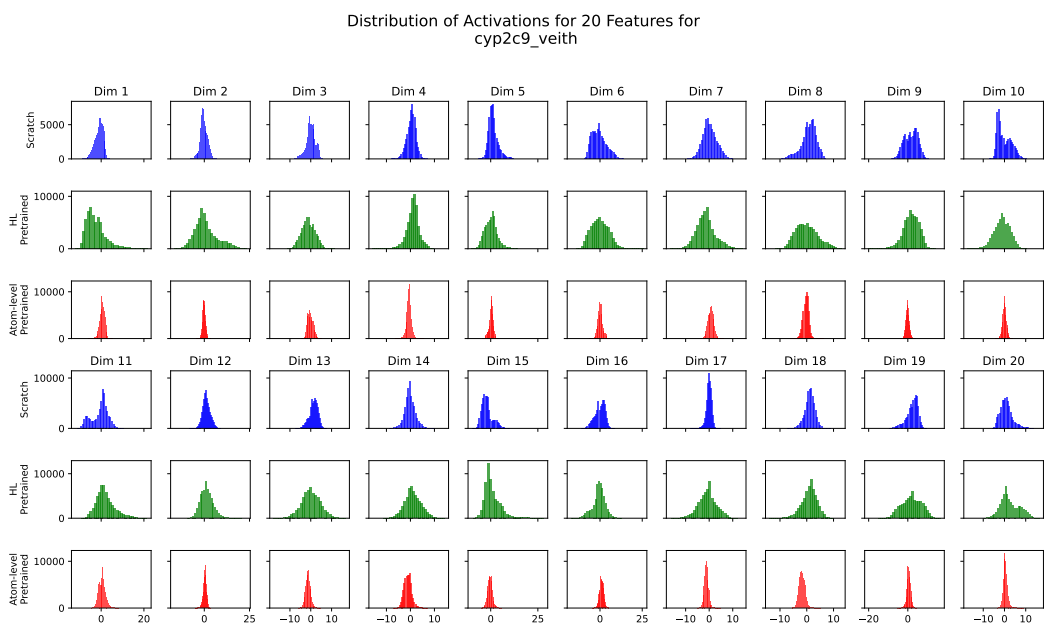


Figure 16: Distribution of first 20 features from the first layer of the Graphormer network for three different training approaches —scratch, HOMO-LUMO pretrained and atom-level pretrained— across test split of cyp2c9 veith dataset.

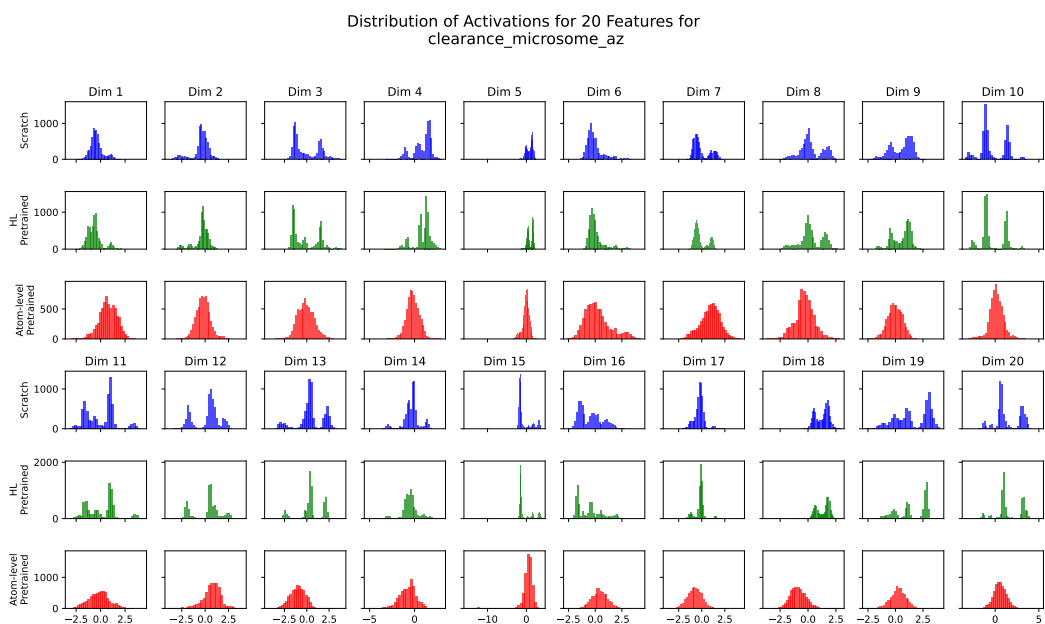


Figure 17: Distribution of first 20 features from the first layer of the Graphormer network for three different training approaches —scratch, HOMO-LUMO pretrained and atom-level pretrained— across test split of clearance microsome az dataset.

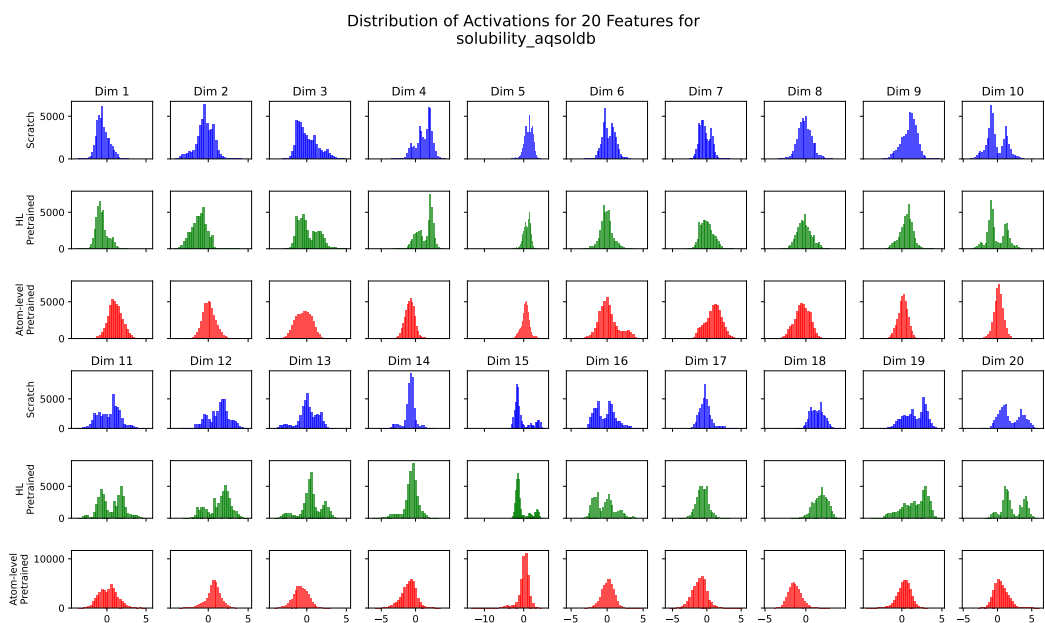


Figure 18: Distribution of first 20 features from the first layer of the Graphormer network for three different training approaches —scratch, HOMO-LUMO pretrained and atom-level pretrained— across test split of solubility aqsolddb dataset.

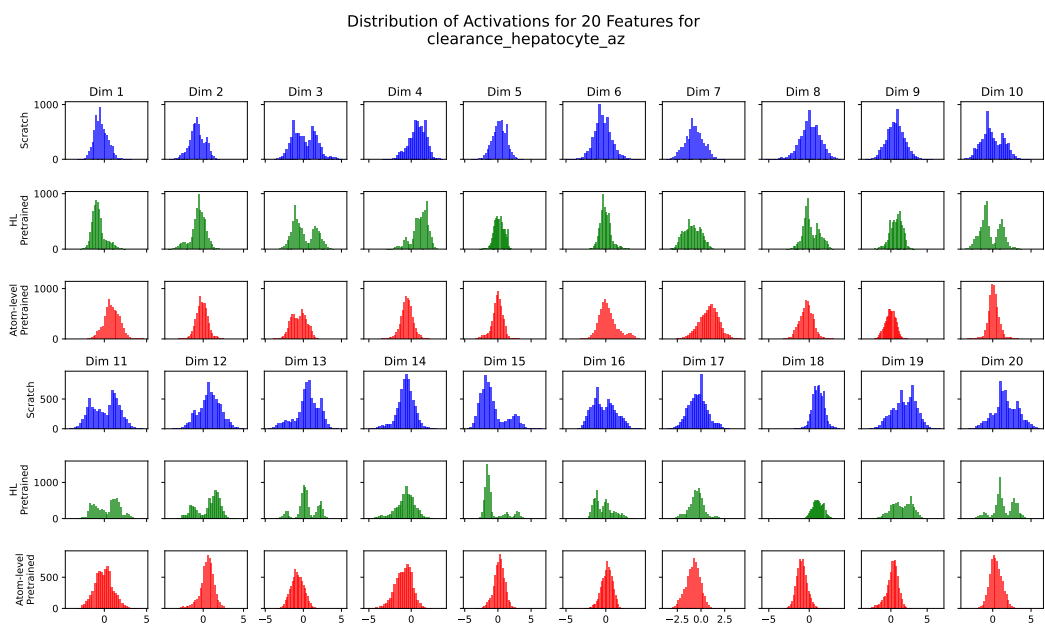


Figure 19: Distribution of first 20 features from the first layer of the Graphormer network for three different training approaches —scratch, HOMO-LUMO pretrained and atom-level pretrained— across test split of clearance hepatocyte az dataset.

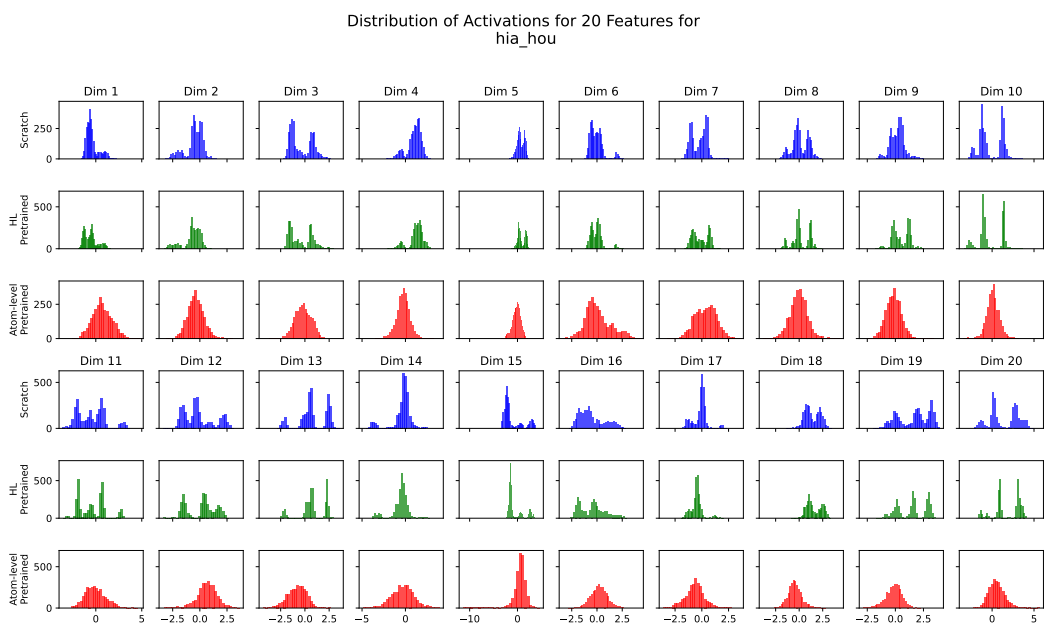


Figure 20: Distribution of first 20 features from the first layer of the Graphormer network for three different training approaches —scratch, HOMO-LUMO pretrained and atom-level pretrained— across test split of hia hou dataset.

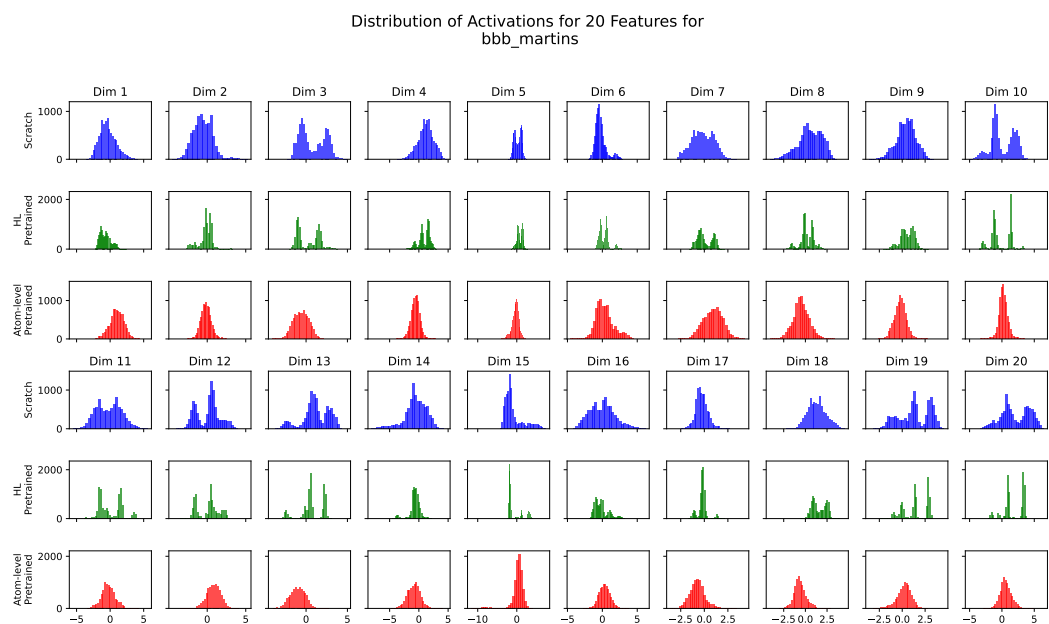


Figure 21: Distribution of first 20 features from the first layer of the Graphormer network for three different training approaches —scratch, HOMO-LUMO pretrained and atom-level pretrained— across test split of bbb martins dataset.

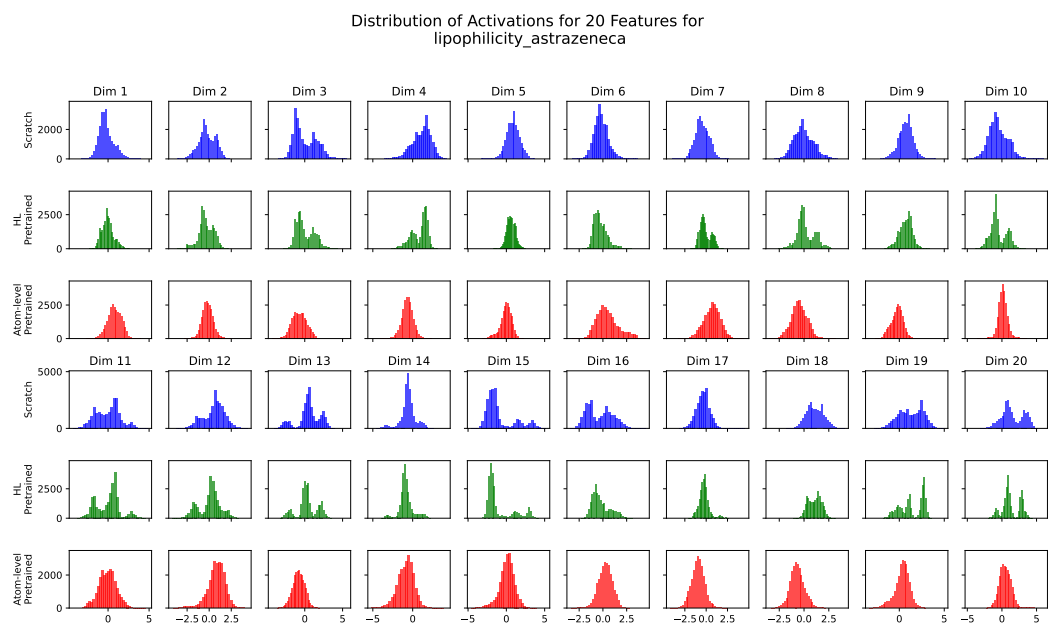


Figure 22: Distribution of first 20 features from the first layer of the Graphormer network for three different training approaches —scratch, HOMO-LUMO pretrained and atom-level pretrained— across test split of lipophilicity astrazeneca dataset.

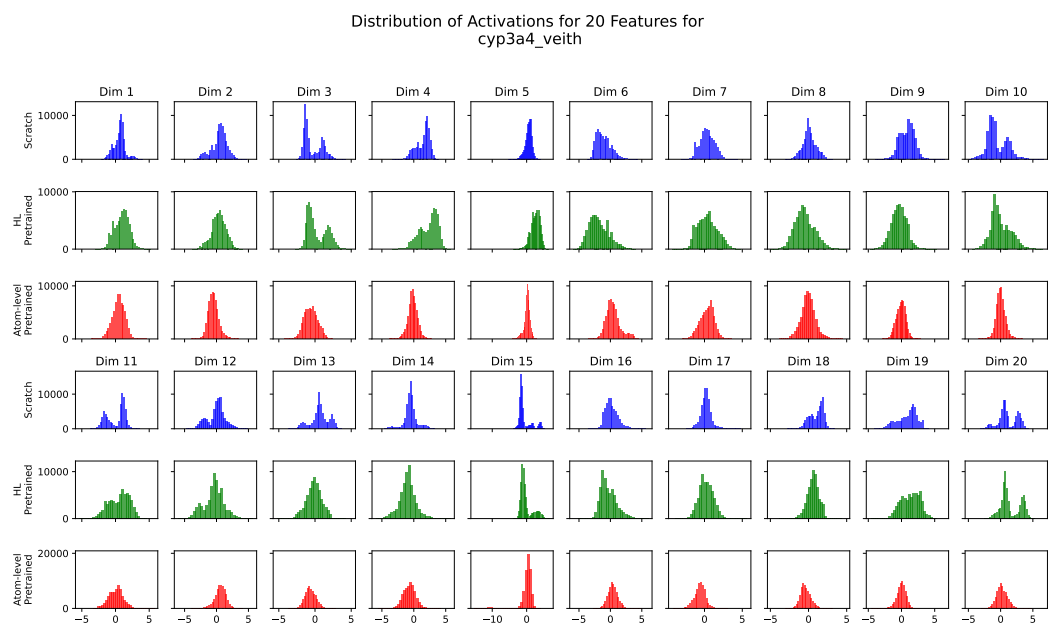


Figure 23: Distribution of first 20 features from the first layer of the Graphormer network for three different training approaches —scratch, HOMO-LUMO pretrained and atom-level pretrained— across test split of cyp3a4 veith dataset.

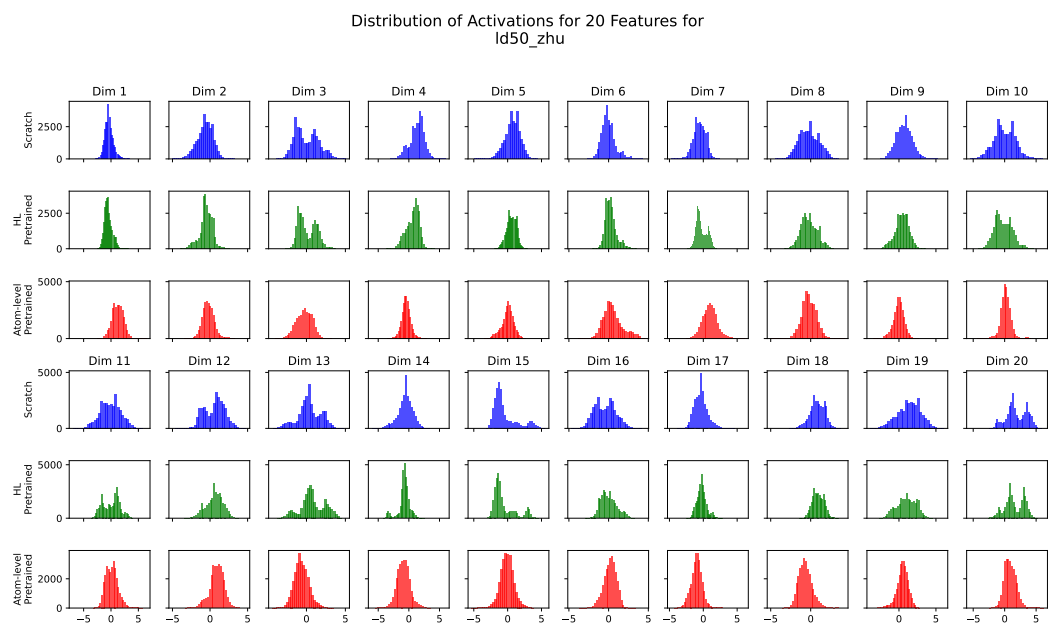


Figure 24: Distribution of first 20 features from the first layer of the Graphormer network for three different training approaches —scratch, HOMO-LUMO pretrained and atom-level pretrained— across test split of ld50 zhu dataset.

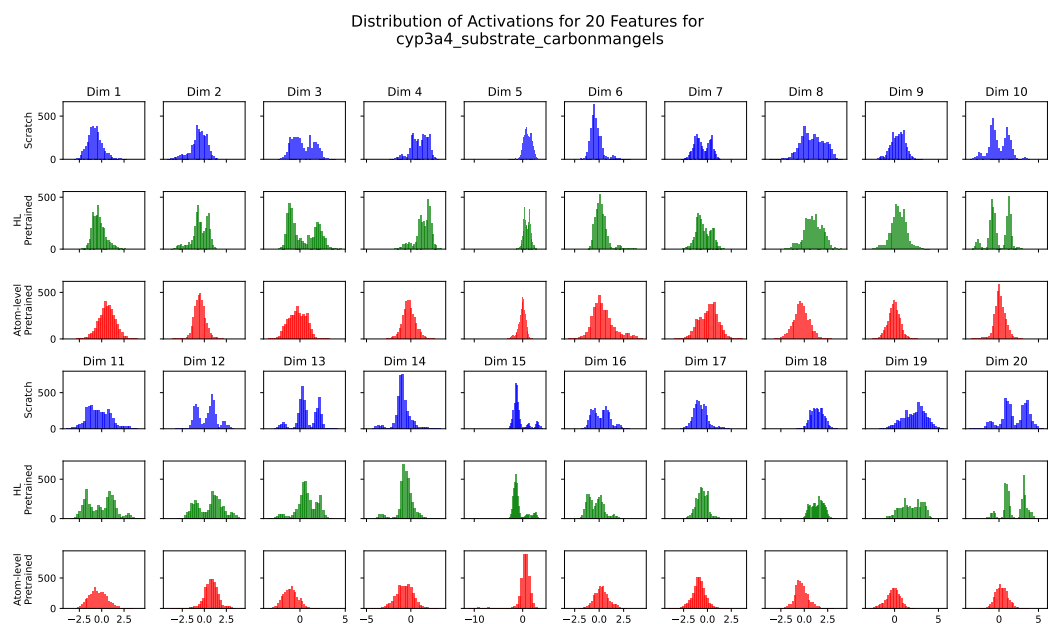


Figure 25: Distribution of first 20 features from the first layer of the Graphormer network for three different training approaches —scratch, HOMO-LUMO pretrained and atom-level pretrained— across test split of cyp3a4 substrate carbonmangels dataset.

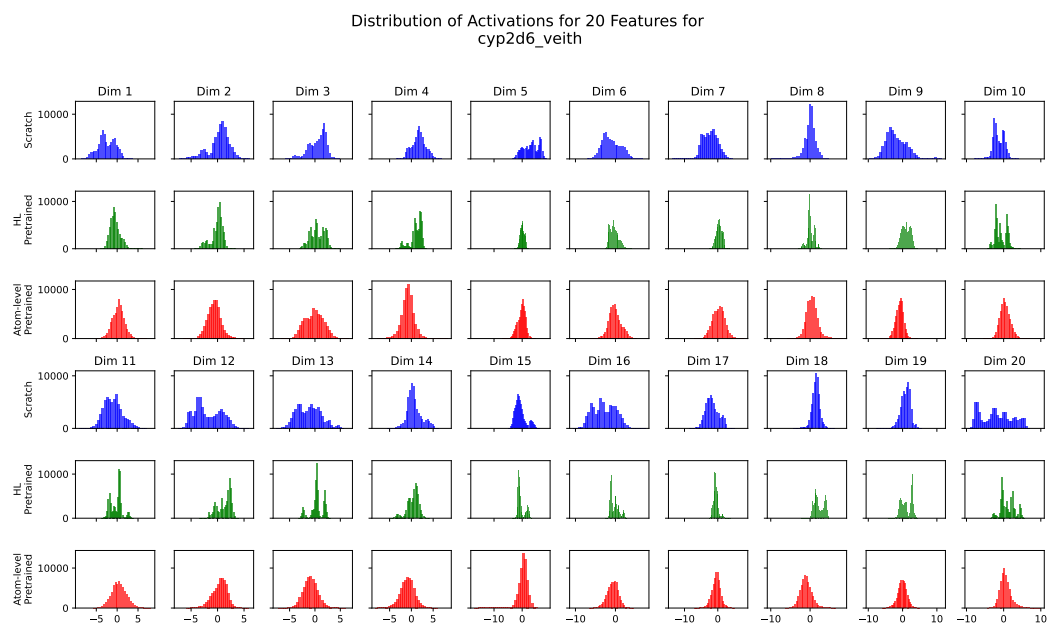


Figure 26: Distribution of first 20 features from the first layer of the Graphormer network for three different training approaches —scratch, HOMO-LUMO pretrained and atom-level pretrained— across test split of cyp2d6 veith dataset.

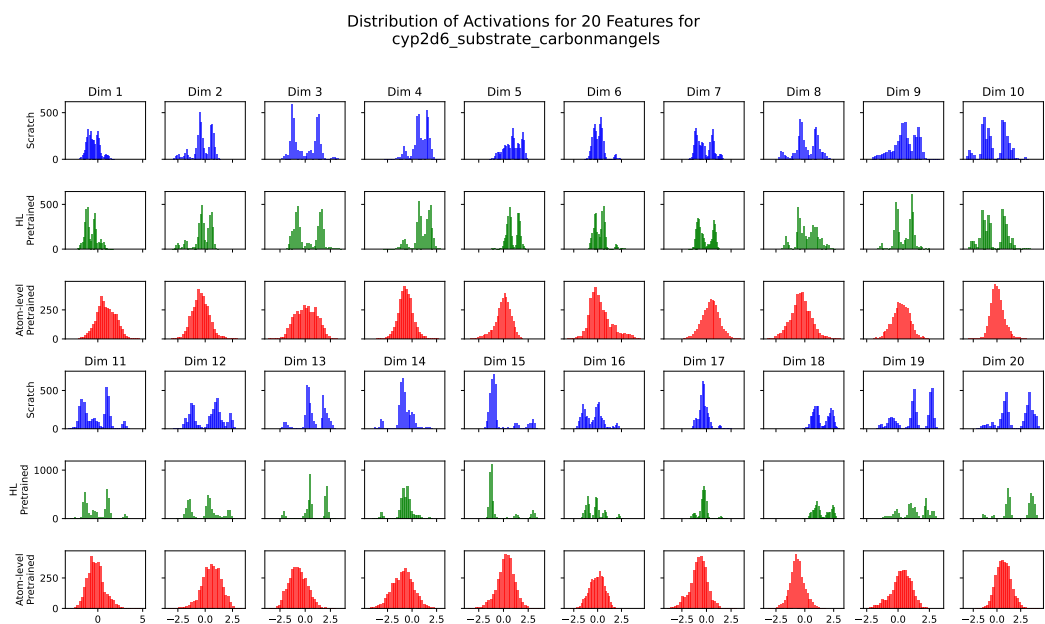


Figure 27: Distribution of first 20 features from the first layer of the Graphormer network for three different training approaches —scratch, HOMO-LUMO pretrained and atom-level pretrained— across test split of cyp2d6 substrate carbonmangels dataset.

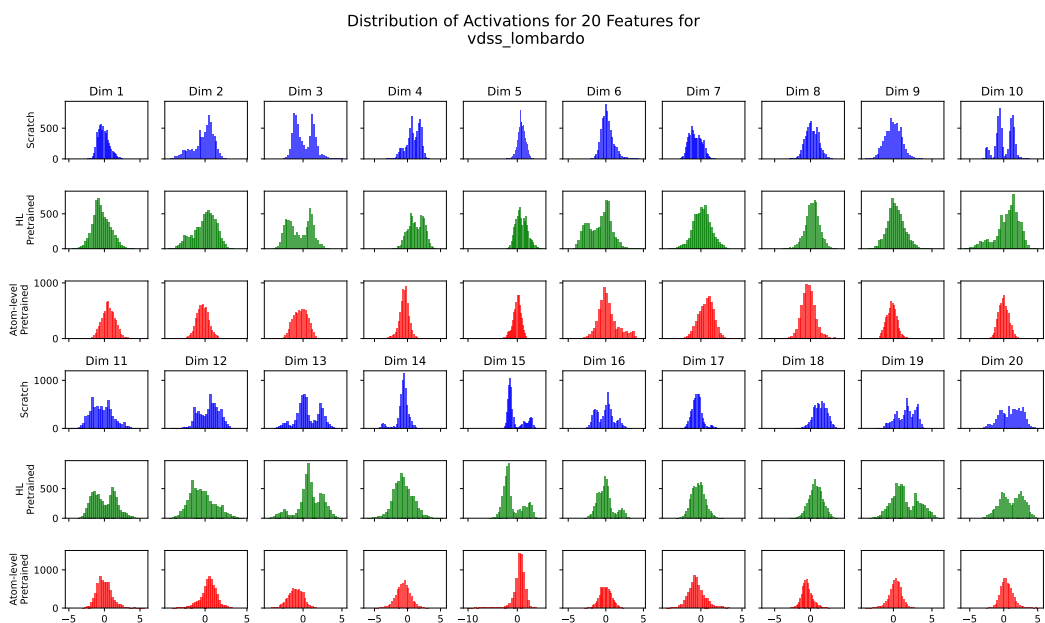


Figure 28: Distribution of first 20 features from the first layer of the Graphormer network for three different training approaches —scratch, HOMO-LUMO pretrained and atom-level pretrained— across test split of vdss lombardo dataset.